Scanning ion conductance microscopy measurement of paracellular channel conductance in tight junctions

Chiao-Chen Chen[1], Yi Zhou[1], Celeste A. Morris[1], Jianghui Hou[2,3*] and Lane A. Baker[1*]

[1]Department of Chemistry, Indiana University, 800 E. Kirkwood Avenue, Bloomington, Indiana 47405;
[2]Renal Division, Washington University Medical School, 660 South Euclid Avenue, St. Louis, Missouri 63110.
[3]Center for Investigation of Membrane Excitability Diseases, Washington University Medical School, 660 South Euclid Avenue, St Louis, Missouri 63110.

Chemicals and Reagents

All solutions were prepared with deionized water (resistivity = 18 MΩ·cm) from a Milli-Q water purification system (Millipore Corp., Danvers, MA) unless otherwise stated. Sodium hypochlorite (10-15% active chlorine, Sigma, St. Louis, MO) and 1 M sodium iodide (Mallinckrodt, Philipsburg, NJ) were utilized for preparation of nanopore membranes as described previously.[1] Potassium chloride (100 mM) (Mallinckrodt, Philipsburg, NJ) and phosphate buffered saline (PBS) (137 mM NaCl, 8.2 mM Na_2HPO_4, 1.8 mM KH_2PO_4, 2.7 mM KCl, pH 7.4) were passed through a 0.22 μm syringe filter (PVDF membrane, Millipore Corp., Danvers, MA) before use. Sodium gluconate (NaGlu, Sigma-Aldrich, St. Louis, MO) and N-methyl-D-glucamine chloride (NMDG·Cl), prepared by titration of N-methyl-D-glucamine (Sigma-Aldrich, St. Louis, MO) to pH 7.4 with hydrogen chloride, were utilized in ion replacement experiments.

Nanopipette Fabrication

Nanopipettes utilized in this study were fabricated from theta quartz capillaries (QT120-90-7.5, Sutter Instrument, Novato, CA) with a CO_2-laser puller (P-2000, Sutter Instrument, Novato, CA) and following the parameters: *Heat = 825, Fil = 3, Vel = 40, Del = 220, Pull = 190.* Tip sizes of the nanopipettes utilized were characterized by imaging Au/Pd-coated specimens with scanning electron microscopy (SEM, FEI Quanta-FEG) as shown in Figure S-1a. The inner diameter of each barrel was determined to be 52 ± 15 nm from 5 pipettes. Both barrels of the theta pipette were

filled with electrolyte (100 mM KCl for polymer membrane experiments or PBS for epithelial monolayer experiments) and individual Ag/AgCl electrodes were inserted into each barrel to construct the scanning probe.

Preparation of Nanopore Membranes

Nanoporous membranes, which serve as a simplified biophysical model of epithelia, were prepared from ion-tracked polyimide membranes (track density 10^6 tracks/cm^2, it4ip, Belgium) via the track-etch process[1]. Careful control of the development conditions, which include pH, temperature, time and concentration of etchant, resulted in nanopores with various dimensions and diameters. In this study, a porous membrane with an average pore radius of 265 ± 20 nm (n=34, characterized by SEM) was utilized (Figure S-1b). The prepared membrane was mounted between two chambers of a conductivity cell with an exposed area of 0.008 cm^2 to allow the membrane to contact electrolyte from both sides.

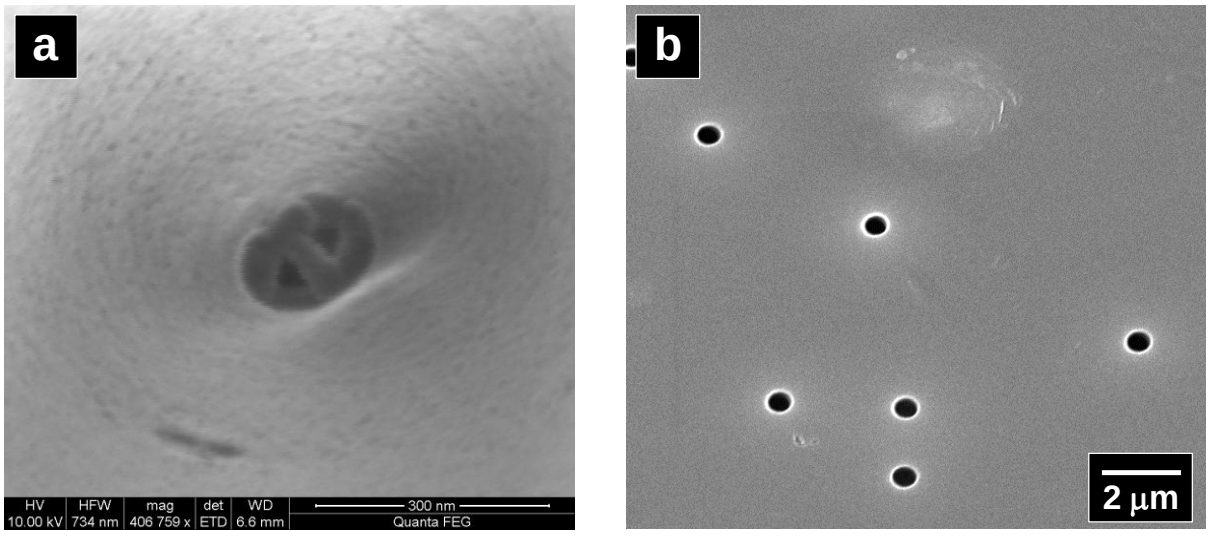

Figure S-1. SEM images of (a) the end-on view of a theta nanopipette with an inner diameter of 54 nm and (b) the polymer membrane with an average pore diameter of 264 ± 20 nm (n=34) utilized in this study.

Immunolabeling and Confocal Microscopy

Cells grown on Transwell inserts (Corning) were fixed with cold methanol (-20°C), followed by blocking with phosphate-buffered saline containing 10% fetal bovine serum and incubation with primary antibodies (1:300) and fluorescein isothiocyanate

(FITC) -labeled secondary antibodies (1:200) as described previously.[2] After washing with phosphate-buffered saline, slides were mounted with Mowiol (Calbiochem). Confocal analyses were performed using the Nikon TE2000 confocal microscopy system equipped with Plan-Neofluar ×40 (numeric aperture 1.3 oil) and ×63 (numeric aperture 1.4 oil) objectives and krypton-argon laser (488 lines). Emissions from FITC were detected with the band-pass FITC filter set of 500–550 nm. All images were converted to JPEG format and arranged using Photoshop CS5 (Adobe).

Molecular Cloning and Retrovirus Production

Hairpin oligonucleotides (siRNA) against the dog claudin-2 gene were synthesized by Integrated DNA Technologies (Coralville, IA) and subsequently annealed and cloned into the Moloney murine leukemia virus retrovirus backbone downstream of the human small nuclear RNA U6 promoter to create the pSIREN-claudin siRNA constructs as described before.[2] Vesicular stomatitis virus glycoprotein (VSV-G) pseudotyped retroviruses were produced in HEK293T cells and used to infect MDCKII cells at a titer of 1×10^6 colony-forming units/ml, as described previously.[3]

Protein Electrophoresis and Immunoblotting

Confluent cells were dissolved in lysis buffer (50 mM Tris-HCl, pH 7.5, 150 Mm NaCl, 1% SDS, and protease inhibitor mixture; Pierce). After shearing with a 23-gauge needle, lysates (containing 15 μg of total protein) were subjected to SDS-PAGE under denaturing conditions and transferred to a nitrocellulose membrane followed by blocking with 3% nonfat milk, incubation with primary antibodies (1:1,000) and the horseradish peroxidase-labeled secondary antibody (1:5000), and exposure to an ECL Hyperfilm (Amersham Biosciences), as described previously.[2] Molecular mass was determined relative to protein markers (Bio-Rad).

Alternating Current (AC) Impedance Measurements.

AC impedance analysis (CHI 660C potentiostat, CH Instruments, Austin, TX) was utilized to assess the epithelial properties of cell monolayers prepared in this study. Measurements of transepithelial impedances were performed on the cell monolayers with an excitation signal of 20 mV (peak-to-peak) sinusoidal alternating potential at 60 discrete frequencies from 1 Hz to 100k Hz (**Figure S-2a**). The resultant impedance

was analyzed from a Nyquist plot in which the imaginary portion of the impedance, Z_{im}, was plotted as a function of the real portion of the impedance, Z_{re}.[4] For a confluent monolayer of uniform cells, a semicircular response was observed. Equivalent circuit analysis of a simple "lumped" model, valid for unilayered epithelia with open lateral spaces, was used.[5-7] In this model, the electrophysiological properties of epithelia are described as a parallel circuit of an epithelial resister (R^e) and a membrane capacitor (C^e), in series with an additional resistor, which represents any ohmic non-epithelial contribution to the transepithelial resistance (TER, R^t). From a Nyquist plot, R^t and the subepithelial resistance (R^{sub}) can be determined by extrapolation of the low and high frequency ends of the impedance locus to the abscissa, respectively. Consequently, impedance measurement allows the discrimination between R^e ($R^e = R^t - R^{sub}$) and R^{sub}. The membrane capacitance (C^e) also can be determined from the frequency at which $|Z_{im}|$ reaches a maximum ($C^e = 1/(\omega_{|Z_{im}|_{max}} \times R^e)$).[8]

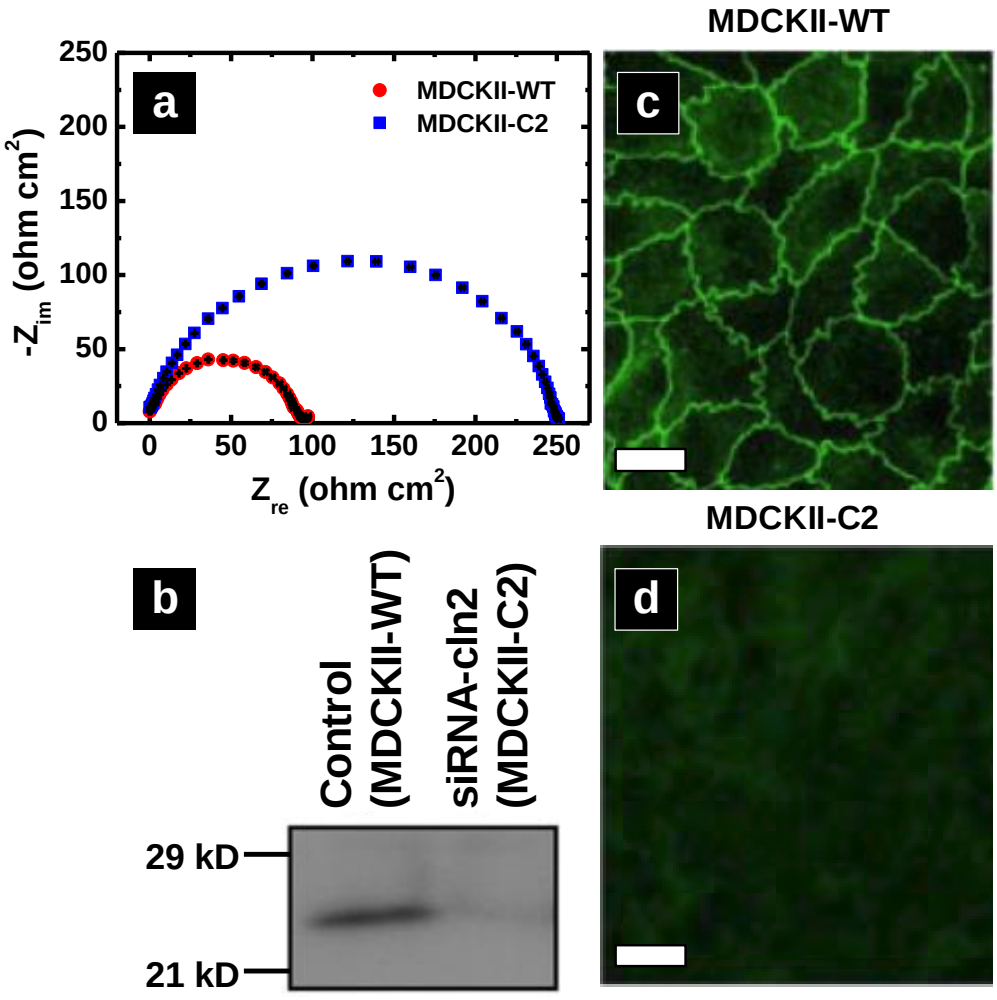

Figure S-2. (a) AC impedance measurements, (b) Western immunoblots and (c-d) confocal fluorescence microscopic images for MDCKII-WT and MDCKII-C2 monolayers demonstrated correlation between the epithelial permeability with the expression of claudin-2, a tight junction protein that was believed to implicate increased permeability of epithelial tissues. (d) MDCKII-C2 cells with deficient claudin-2 expression were immunostained and revealed >95% loss of fluorescent intensity as compared to MDCKII-WT cells. Scale bar: 5 μm.

Linearity of Epithelial Cell Monolayers

To analyze impedance measurements with the equivalent electrical circuit composed of linear components, the linearity of epithelial monolayers utilized here must be verified, as shown in **Figure S-3**. The recorded I-V responses demonstrate that, within the range of the potential tested, the amplitude of the transepithelial potential applied for impedance analysis, and the subsequent conductance measurement with SICM does not affect the epithelial resistance (conductance) under study.[9, 10]

Current-voltage responses of the whole epithelial cell monolayers were characterized with linear sweep voltammetry (CHI 660C potentiostat, CH Instruments, Austin, TX). The resultant current-voltage curves were utilized to examine the effects of applied transepithelial potential to the transepithelial resistance (TER), which is an index to characterize the integrity of epithelial monolayers. Within the test range of -50 mV to +50 mV, a linear relationship was observed for both MDCKII-WT and MDCKII-C2 cell monolayers. This observation demonstrated that within the tested range, the transepithelial potential applied did not alter the epithelial resistance (conductance) under study. Therefore, both the impedance analysis and the subsequent conductance measurement with P-SICM were performed with a transmembrane potential no larger than 50 mV to insure the measurements obtained were from an intact epithelial system.

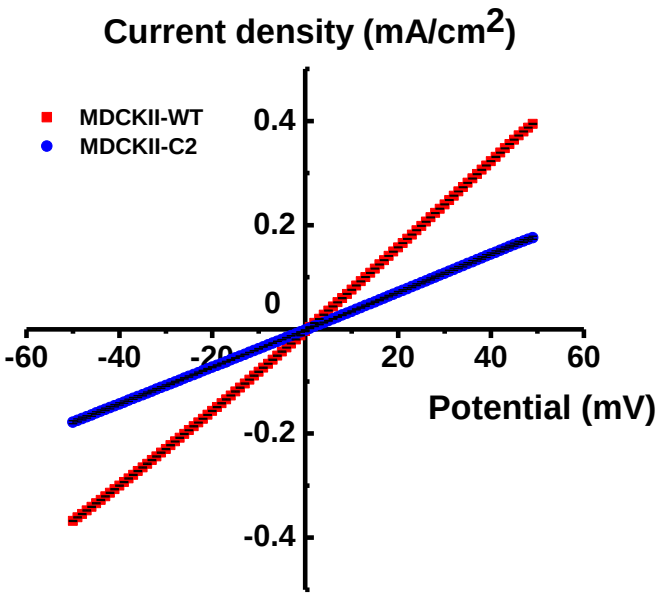

Figure S-3. Current-voltage responses of a representative MDCKII-WT (■) and a representative MDCKII-C2 (●) cell monolayers were recorded. Positive potential refers to the positivity of the voltage applied to the apical compartment of a culture insert with respect to that applied to the basolateral chamber. These I-V relationships were linear in the range explored (± 50 mV).

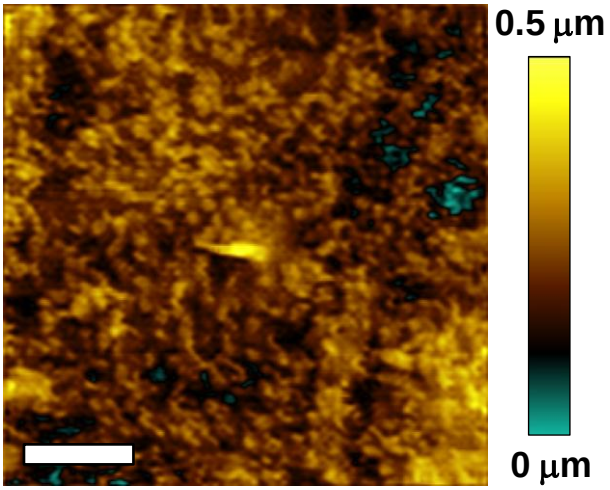

Figure S-4. The high resolution image of the apical surface of MDCKII-WT cells which shows the subcellular structures, namely microvilli, on epithelial membrane surfaces. This observation demonstrates the high spatial resolution that can be achieved with P-SICM, and thus confirms the capability of the method to perform local conductance measurements on the nanometer scale. Scale bar: 2 μm.

Effects of Probe Size on Local Potential Measurement

Localized potential variations, a result of inhomogeneous conductivity in a permeable membrane, were recorded for a series of transmembrane potentials (V_{TM}). Two pores in close proximity were examined under these conditions with two theta scanning probes with different tip sizes. From to the pipette resistances measured, the tip sizes of one barrel of these theta pipettes were estimated to be ~30 nm and ~100 nm, respectively. The intensity of resultant potential images were plotted as a function of applied transmembrane potentials as shown in **Figure S-5a**. Here, under the same conditions (i.e. same pores and applied V_{WE}), potential images with greater intensity, which implies steeper changes in the local potential, were observed with the theta probe with a smaller tip. We have demonstrated in our previous studies that scanning probes with smaller tip size provided a closer probe-surface distance (D_{ps}) for imaging.[11] And thus the results obtained here demonstrate that a theta pipette with a smaller tip size allowed to image in a closer proximity of the membrane surface where the changes in local potential is steeper. Consequently, a better discrimination between conductive pathways and impermeable areas was achieved from the potential measurements with a smaller probe.

However, limited by increase in the pipette resistance, when a smaller probe was utilized, the current measurements obtained simultaneously with potential measurements did not show increase in the intensity of recorded current images, even though the measurements were performed at a smaller D_{ps}. In contrary, a decrease in the current magnitude was observed for each applied V_{WE}, as compared to that obtained with a larger tip (**Figure S-5b**). These results further demonstrate the advantages offered by potential measurements as compared to current measurements. In addition to improved signal-to-noise ratio, potential measurements allow examination with a smaller probe, which provides a better spatial resolution without sacrifice of detection sensitivity.

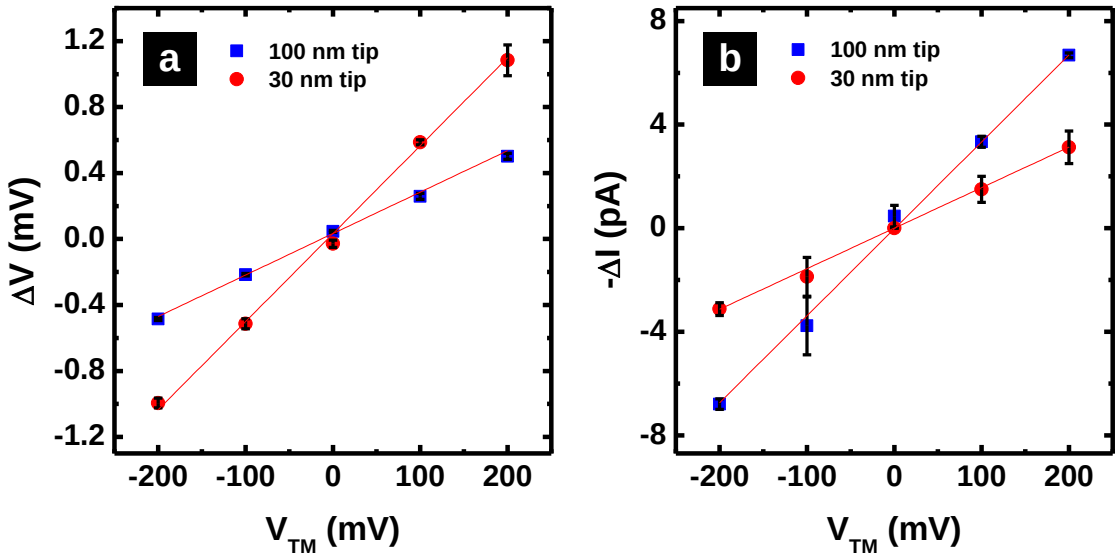

Figure S-5. The intensity of the (a) potential images and the (b) ion current images were plotted as a function of the applied transmembrane potentials (V_{TM}). These measurements were recorded with two theta pipettes with tip sizes (each barrel) of ~ 30 nm (red circle) and ~ 100 nm (blue square), respectively, to assess the effects of the probe size on the resultant potential and current measurements.

Table S-1.

Descriptive statistics of Shapiro-Wilk test* for normality assessment of conductance measurements shown in Figure 4.

Local conductance (G)	Sample size	Mean (mS/cm^2)	Standard deviation (mS/cm^2)	*p*-value**	Normal distribution
MDCKII-WT_over CB	49	2.52635	1.48564	0.09834	Yes
MDCKII-WT_over CJ	62	6.19693	2.53974	0.76907	Yes
MDCKII-C2_over CB	67	1.54355	0.91075	0.02390	No
MDCKII-C2_over CJ	78	2.63119	1.26126	0.24109	Yes

* The alpha level for Shapiro-Wilk test is 0.05.

** *p*-vlaue > 0.05 indicates the data from a normally distributed population.

Table S-2.

Statistical analysis of difference between conductance measurements of two groups shown in Figure 4c.

Data sets	Statistical test*	*p*-value**
MDCKII-WT_over CB vs. MDCKII-WT_over CJ	two-sample t-test	9.4448E-15
MDCKII-WT_over CJ vs. MDCKII-C2_over CJ	two-sample t-test	3.4811E-20
MDCKII-C2_over CB vs. MDCKII-C2_over CJ	Mann-Whitney test	1.5990E-7
MDCKII-C2_over CB vs. MDCKII-WT_over CB	Mann-Whitney test	5.7520E-4

* The alpha level for the independent two-sample t-test and the Mann-Whitney test is 0.05.

** *p*-vlaue < 0.05 indicates there is significant difference between two groups.

Table S-3.

Descriptive statistics of Shapiro-Wilk test* for normality assessment of conductance measurements shown in Figure 5.

Cell line	Basolateral buffer	Local conductance (G)	Sample size	Mean (mS/cm^2)	Standard deviation (mS/cm^2)	*p*-value**	Normal distribution
MDCKII-WT	NaCl (control)	over CB	40	3.01310	1.36300	0.12034	Yes
		over CJ	46	6.24335	2.36917	0.34932	Yes
	NMDG·Cl	over CB	44	2.72452	1.21128	0.12134	Yes
		over CJ	53	4.36713	1.76184	0.16049	Yes
	NaCl (control)	over CB	27	3.14615	1.59010	0.61422	Yes
		over CJ	42	6.36488	2.49345	0.38475	Yes
	NaGlu	over CB	36	2.93608	2.11494	0.74187	Yes
		over CJ	42	5.33246	2.24542	0.52211	Yes
MDCKII-C2	NaCl (control)	over CB	34	1.64654	1.00637	0.53615	Yes
		over CJ	32	2.63755	1.40651	0.20426	Yes
	NMDG·Cl	over CB	31	1.60617	0.76246	0.53385	Yes
		over CJ	33	2.45778	1.24076	0.06653	Yes
	NaCl (control)	over CB	33	1.71042	0.94871	0.05135	Yes
		over CJ	33	2.75368	1.22650	0.83299	Yes
	NaGlu	over CB	41	1.55239	0.87135	0.10118	Yes
		over CJ	41	2.61531	1.00495	0.77349	Yes

* The alpha level for Shapiro-Wilk test is 0.05.

** *p*-vlaue > 0.05 indicates the data from a normally distributed population.

Table S-4.

Statistical analysis of difference between conductance measurements of two groups shown in Figure 5.

Cell line	Data sets	Statistical test*	*p*-value**
MDCKII-WT	NaCl (control) over CB vs. NMDG·Cl over CB	two-sample t-test	0.30725
	NaCl (control) over CJ vs. NMDG·Cl over CJ	two-sample t-test	1.8397E-5
	NaCl (control) over CB vs. NaGlu over CB	two-sample t-test	0.66709
	NaCl (control) over CJ vs. NaGlu over CJ	two-sample t-test	0.04948
MDCKII-C2	NaCl (control) over CB vs. NMDG·Cl over CB	two-sample t-test	0.857
	NaCl (control) over CJ vs. NMDG·Cl over CJ	two-sample t-test	0.46046
	NaCl (control) over CB vs. NaGlu over CB	two-sample t-test	0.45846
	NaCl (control) over CJ vs. NaGlu over CJ	two-sample t-test	0.59528

* The alpha level for the independent two-sample t-test is 0.05.

** *p*-vlaue < 0.05 indicates there is significant difference between two groups.

References

(1) Fleischer, R. L.; Price, P. B.; Walker, R. M. *Nuclear Tracks in Solids. Principles and Applications*; Univ. of California Press: Berkeley, 1975.

(2) Hou, J.; Gomes, A. S.; Paul, D. L.; Goodenough, D. A. *J. Biol. Chem.* **2006**, *281*, 36117-36123.

(3) Hou, J.; Paul, D. L.; Goodenough, D. A. *J. Cell Sci.* **2005**, *118*, 5109-5118.

(4) Bard, A. J.; Faulkner, L. R. In *Electrochemical Methods: Fundamentals and Applications,* 2 ed.; John Wiley & Sons, Hoboken, NJ, USA: Hoboken, NJ, USA, 2001, pp 368-416.

(5) Teorell, T.; WersÄLl, R. *Acta Physiol. Scand.* **1945**, *10*, 243-257.

(6) Schifferdecker, E.; Fromter, E. *Pfluegers Arch. - Eur. J. Physiol.* **1978**, *377*, 125-133.

(7) Wills, N. K.; Reuss, L.; Lewis, S. A. *Epithelial Transport: A Guide to Methods and Experimental Analysis*; Springer, 1996.

(8) Krug, S. M.; Fromm, M.; Guenzel, D. *Biophys. J.* **2009**, *97*, 2202-2211.

(9) CIausen, C. *Methods Enzymol.* **1989**, *171*, 628-642.

(10) Gitter, A. H.; Bertog, M.; Schulzke, J. D.; Fromm, M. *Pfluegers Arch. - Eur. J. Physiol.* **1997**, *434*, 830-840.

(11) Chen, C.-C.; Baker, L. A. *Analyst* **2011**, *136*, 90-97.